

Addimer chain structures: Metastable precursors to island formation on Ge–Si(001)-(2 × n) alloyed surface

Kyle J. Solis^a, Lance R. Williams^b, B.S. Swartzentruber^c, Sang M. Han^{a,*}

^a Department of Chemical and Nuclear Engineering, University of New Mexico, Albuquerque, NM 87131, United States

^b Computer Science Department, University of New Mexico, Albuquerque, NM 87131, United States

^c Sandia National Laboratories, Albuquerque, NM 87185, United States

Received 24 July 2006; accepted for publication 8 September 2006

Available online 29 September 2006

Abstract

We have identified addimer chain structures as metastable precursors to compact epitaxial islands on the (2 × n) reconstructed SiGe wetting layer, using polarity-switching scanning tunneling microscopy (STM). These chain structures are comprised of 2–12 addimers residing in the troughs of neighboring substrate dimer rows. The chain structures extend along equivalent $\langle 1\ 30 \rangle$ directions across the substrate dimer rows in a zigzag fashion, giving rise to kinked and straight segments. We measure a kink-to-straight ratio of nearly 2:1. This ratio corresponds to a free energy difference of 17 ± 4 meV, favoring the formation of kinked segments. The chain structures convert to compact epitaxial islands at elevated temperatures (≥ 90 °C). This conversion suggests that the chain structures are a precursor for compact island formation on the SiGe wetting layer. We digitally process filled- and empty-state STM images to distinguish chain structures from compact islands. By monitoring the populations of both species over time, the chain-to-island conversion rates are measured at substrate temperatures ranging from 90 to 150 °C. The activation energy for the conversion process is measured to be 0.7 ± 0.2 eV with a corresponding pre-exponential factor of $5 \times 10^{4 \pm 2} \text{ s}^{-1}$.

© 2006 Elsevier B.V. All rights reserved.

Keywords: Addimer chain structures; Compact epitaxial islands; C-dimer; Polarity-switching scanning tunneling microscopy; (2 × n) Silicon–germanium alloy; Surface kinetics

1. Introduction

The lattice mismatch of 4.2% in the Ge–Si heterosystem gives rise to a significant amount of strain at the interface. This misfit strain, in turn, manifests itself structurally and electronically, ultimately influencing device performance. Some of the positive effects include an increase in charge carrier mobility, quantum structure formation, and band-gap alteration [1–5]. These desirable attributes lend SiGe technology to a diverse range of microelectronic [2,6–9] and optoelectronic device applications [10–12]. However, the strain can cause an increase in the density of defects and dislocations adversely affecting the performance of

such devices [1,13]. The remaining engineering challenge is to take advantage of the numerous intrinsic benefits of this system, while mitigating the negative effects.

Many of the aforementioned applications require highly selective growth of $\text{Si}_{1-x}\text{Ge}_x$ ($0 \leq x \leq 1$) and precise control over size and spatial distributions at the nanoscale. In order to gain such selectivity and controllability, we study the surface processes responsible for heteroepitaxial film growth at the atomic-level. Our interests include identification of the main mass transport species; their interactions with other adspecies and the surface; and the relative stabilities of the various surface adspecies and adstructures. Herein, we specifically focus on the kinetics of compact epitaxial island formation on the Ge–Si(001)-(2 × n) alloyed wetting layer.

The heteroepitaxy of Ge on Si(001) is a model example of the Stranski–Krastanov growth mode, in which a

* Corresponding author. Tel.: +1 505 277 3118; fax: +1 505 277 5433.
E-mail address: meister@unm.edu (S.M. Han).

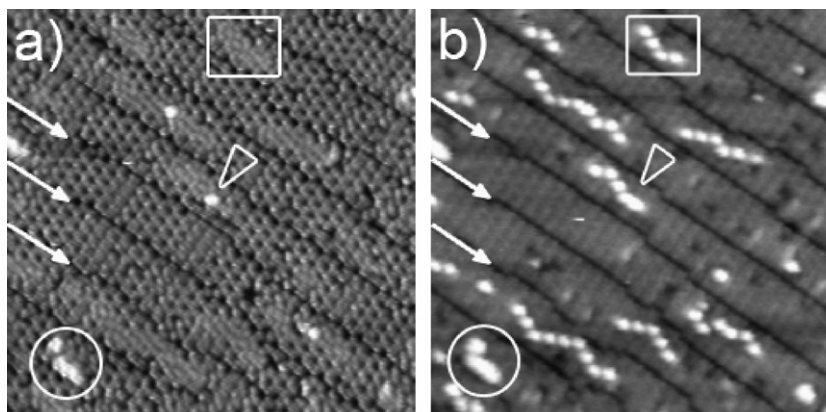


Fig. 1. STM images ($200 \text{ \AA} \times 200 \text{ \AA}$) of the $(2 \times n)$ reconstructed SiGe wetting layer. The dimer vacancy lines are seen to run across the images at $\sim 45^\circ$ angle. Three vacancy lines are identified by white arrows. (a) Filled-state image (-1.7 V) showing a highly buckled, “honeycomb-like”, $c(4 \times 2)$ surface and very little apparent surface adspecies shown as white features. Note that the faint “ghost-like” areas of disturbed substrate dimers, outlined by a white rectangle, correspond to the presence of ADCSs which are easily seen in (b) a corresponding empty-state image ($+1.7 \text{ V}$). Epitaxial islands are clearly visible in the lower left corner in both biases outlined by a white circle. The triangle identifies a C-dimer in a linear structure.

pseudomorphic two-dimensional wetting layer is initially formed, followed by the nucleation and growth of three-dimensional islands. Upon Ge exposure, a clean Si(001)- (2×1) surface is transformed into an alloyed SiGe wetting layer, exhibiting a $(2 \times n)$ reconstruction (see Fig. 1) [14–17]. For this particular reconstruction, every n th dimer is missing from the surface, forming long-range ordered dimer vacancy lines which extend perpendicular to the substrate dimer rows. These vacancy lines, identified by white arrows in Fig. 1, decrease misfit stress by allowing the compressed substrate dimers to relax outwards. This $(2 \times n)$ alloyed surface serves as the substrate for this study.

Addimer chain structures (ADCSs) have been observed previously as metastable adspecies on Si(001) exposed to Si [18,19], Si(001) exposed to Ge [20], Ge(001) exposed to Si [21] and Ge(001) exposed to Ge [22,23]. We have similarly identified ADCSs on the SiGe alloy surface upon sub-monolayer (sub-ML) Ge deposition at room temperature. We further observe the transition of these chain structures into compact epitaxial islands. This transition suggests that ADCSs are metastable precursors during epitaxial growth on the alloy surface. The purpose of this paper is to characterize the mobility, configurational energetics, and activation energy associated with the transition of these metastable ADCSs to compact islands, thereby providing additional information on the early stages of epitaxial growth on the SiGe alloyed wetting layer.

2. Experimental methods

The experiments are carried out in a UHV chamber (base pressure $\leq 5 \times 10^{-11}$ Torr) equipped with a variable-temperature scanning tunneling microscope (STM) with a chemically etched W tip. Si(001) samples are flash-annealed to $\sim 1250 \text{ }^\circ\text{C}$ for 1 min, then rapidly quenched to room temperature, yielding a (2×1) reconstructed substrate. The $(2 \times n)$ alloy is formed by depositing approxi-

mately 1.5 monolayers (ML) of Ge from a resistively heated W-wire basket while the substrate is held between 500 and 600 $^\circ\text{C}$. This preparation results in a SiGe alloy wetting layer exhibiting $(2 \times n)$ reconstruction with highly ordered dimer vacancy lines. The ADCSs are then formed by sub-ML Ge deposition on the $(2 \times n)$ surface at room temperature. Finally, the sample is transferred to the STM probe stage. Large area ($500 \text{ \AA} \times 500 \text{ \AA}$) dual-polarity scans are then acquired at various locations on the sample at temperatures ranging from 90 to 150 $^\circ\text{C}$. During polarity-switching STM, the STM tip scans from left to right at a negative sample bias (-1.7 V), reverses the substrate bias polarity ($+1.7 \text{ V}$), and scans the same line from right to left. The tip then translates to the next line and repeats this process in a raster fashion until complete filled- and empty-state, constant-current ($\sim 100 \text{ pA}$) images of the surface are acquired simultaneously.

3. Results and discussion

The above procedure results in surfaces like that shown in Fig. 1, which compares filled-state (Fig. 1(a)) and empty-state images (Fig. 1(b)) of the same area. The polarity-switching STM technique is essential to the study of ADCSs as evidenced by the dramatic differences between Fig. 1(a) and (b). For example, while compact islands and *on-top* addimers (white circle) are easily seen in both filled- and empty-state STM images, ADCSs (white rectangle) are only seen easily in empty-state images. In filled-state images, ADCSs are virtually invisible, appearing only as faint “ghost-like” features and cause a change in the buckling phase of the underlying substrate dimers [18,22,23].

For Si(001) and Ge(001) (2×1) surfaces, addimers have been predicted [24–28] and experimentally observed [18,25,26,29,30] to assume any of four possible binding sites shown in Fig. 2. This figure illustrates that addimers can reside *on* a substrate dimer row or *in* a trough, between

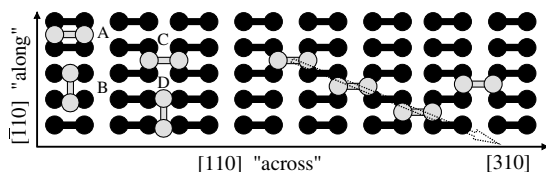


Fig. 2. Various addimer (gray) adsorption sites, orientations and nomenclature for a (2×1) surface (black). Also shown is a four-unit ADCS illustrating the relative positions of the constituent C-dimers with respect to each other and the surface dimers. The use of the terms *along* and *across* with respect to substrate dimer rows correspond to $[\bar{1}10]$ and $[110]$ directions, respectively. The chain structure extending along $[310]$ direction is overlaid with a dotted arrow.

two neighboring dimer rows. Additionally, the addimer bond direction can be parallel to the substrate dimer bonds (A and C) or perpendicular to them (B and D). While all these adsorption sites are local energy minima, they are not equally favorable. For instance, theoretical predictions [24,27,28] for single Si addimers on Si(001) suggest *on-top* dimers (A and B) to be more stable than *in-trough* dimers (C and D). These predictions have been supported by experimental observations [25,30,31] in which *on-top* dimers are more commonly observed than *in-trough* dimers. The relative energies of *on-top* dimers (A and B) are nearly degenerate, although the epitaxial configuration (B) is slightly favored. A low activation barrier allows the addimers to rotate freely between the two configurations at room temperature [26]. As for the less stable *in-trough* dimers, C-dimers are a metastable configuration whose formation is dominated by kinetics [18], while isolated D-dimers have never been observed [18].

However, the relative stabilities of the addimers can change when adstructures, composed of multiple addimers are formed [28]. For instance, two commonly observed adstructures for Ge on the Si(001)- (2×1) surface are dilute dimer rows and compact epitaxial islands [18,27–30,32,33]. The dilute dimer row is a linear arrangement of C-dimers occupying neighboring *in-trough* sites, alternating with vacant *on-top* sites extending across the substrate dimer rows in (110) directions. Compact epitaxial islands are similar to dilute dimer rows, in that they also extend across the substrate dimer rows. However, compact islands do not contain vacant sites and consist of alternating *on-top* and *in-trough* addimers arranged in an epitaxial fashion (i.e., BDBD). Furthermore, annealing treatments demonstrate that compact islands are thermodynamically more stable than dilute dimer rows [33].

The addimer chain structures (ADCSs), as another type of adstructures, are observed on the $(2 \times n)$ SiGe wetting layer. Similar to Ge dilute dimer rows on Si(001), ADCSs are linear structures consisting of C-dimers residing at neighboring *in-trough* sites. However, ADCSs extend along equivalent $\langle 130 \rangle$ directions at $\sim 63^\circ$ with respect to the substrate dimer row orientation (Fig. 1 and dotted arrow in Fig. 2). Another difference is that ADCSs are visible only in empty-state images (Fig. 1), whereas dilute dimer rows

are visible in filled- and empty-state images. We further observe that ADCSs range in length from 2 to approximately 12 units of C-dimers; however, the most commonly observed lengths are 2–5 units. Note that isolated C-dimers also exist as a stable adspecies instead of being a part of the chain structure.

The multiple C-dimers that constitute an ADCS are categorized according to their position in the chain with respect to neighboring C-dimers. The chain structures often contain straight and kinked segments which give rise to a zigzag orientation. A C-dimer is categorized as straight, if a line can be drawn through the subject C-dimer and its two neighboring C-dimers along a $\langle 130 \rangle$ direction. In contrast, a kink is defined as a C-dimer whose neighboring C-dimers do not fall on the same straight line along a $\langle 130 \rangle$ direction. For example, the gray circles in Fig. 3 are kinks, deviating from a single straight line. The striped circle is a straight that maintains a single $\langle 130 \rangle$ direction. The white circles at the chain ends are neither kinks nor straights, since they have only one neighbor.

Another characteristic feature of ADCSs is the kink-to-straight ratio, defined as the total number of observed kinked addimers to the total number of observed straight addimers at a given substrate temperature. If the configurations of these ADCSs were completely random, one would expect a ratio close to 1:1. However, based on a sampling size of ~ 8000 chain structures within the 90–150 °C temperature range, the experimentally observed ratio is very close to 2:1, favoring kinks. This value suggests that the kinked orientation is energetically favored by 17 ± 4 meV. In comparison, this configurational preference is exactly reversed for the Ge on Ge(001) system, where Galea et al. [23] observe chain structures to predominantly occupy a more linear, straight configuration with a corresponding free energy difference of 21 meV.

At the temperatures studied (90–150 °C), ADCSs exhibit extremely localized movement of their constituent C-dimers. The chain structures usually reconfigure in such a way to preserve their $\langle 130 \rangle$ orientations. Similar localized movement is observed for Ge chain structures on Ge(001) [23]. The preservation of $\langle 130 \rangle$ orientations imposes constraints on which and how C-dimers can rearrange. As a prototypical example, the initial chain configuration shown in Fig. 3(a) contains two kinks (2 and 4) and one straight (3). The only potentially mobile dimers, which

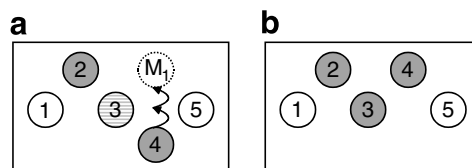


Fig. 3. Schematic defining “ends” (white), “kinks” (gray), and “straights” (striped) according to the relative positions of addimers in an ADCS. After Kink 4 diffuses two lattice sites, indicated by the black arrow in (a), it changes the designation of its neighbor, Dimer 3, from a straight to a kink.

will not disrupt the chain, are the ends (1 and 5) and the kinks (2 and 4). For instance, when Dimer 4 diffuses two lattice sites to its mirror lattice site, M_1 , the configuration becomes that shown in Fig. 3(b). Although Dimer 3's orientation is changed from a straight to a kink, this rearrangement does not disrupt the $\langle 130 \rangle$ orientation of the chain. The reconfigured chain now contains three kinks and no straights. In addition to the typical case, we observe two rare exceptions. One is when a C-dimer cannot diffuse to its mirror lattice site because of surface defects. In this case, the C-dimer will diffuse only one lattice site, resulting in a linear structure along $\langle 110 \rangle$ direction analogous to a dilute dimer row. The C-dimer in this linear structure now appears in both empty- and filled-state images (pointed by a triangle in Fig. 1(a) and (b)). However, this is an unstable configuration for the chain structure, and it quickly assumes the normal $\langle 130 \rangle$ position. The second exception is when an end C-dimer diffuses away from the chain.

To investigate whether confinement of the dimer chain structures between the vacancy lines is responsible for the preference of kinks, we performed Monte Carlo simulations of the dimer chain dynamics. We varied the length of the dimer chain structures and the value of n for the $(2 \times n)$ structure, i.e., the spacing between the vacancy lines. The chain was allowed to reconfigure according to the rules described above, while preserving $\langle 130 \rangle$ orientations. Only for the unphysical case of very tight confinement ($n \leq 4$) and very long chain lengths did the resulting kink-to-straight ratio approach the measured value of $\sim 2:1$. Therefore, the free energy difference between the kinked and straight segments of the dimer chains must predominantly be due to their difference in configuration energy. We speculate that the interaction between the dimer chains and the arrangement of the underlying substrate dimers results in the observed preference for kinks.

In addition to the rearrangement of ADCS via diffusion of their constituent addimers, we have observed the transi-

tion of these diluted chain structures into compact epitaxial islands. The term “diluted” refers to the fact that ADCSs, like dilute dimer rows, occupy only *in-trough* sites and not *on-top* sites. The STM images (before/after) in Fig. 4 are taken from a movie and capture such a transition. Fig. 4(a) and (b) are filled- and empty-state images of a six-unit ADCS, respectively. The chain structure is characteristically seen only in the empty-state image. However, after the ADCS collapses into two compact epitaxial segments, these islands are easily seen in both polarities (Fig. 4(c) and (d)). Since the conversion to compact islands is a thermally activated process, we measure the conversion rate as a function of temperature to calculate the associated activation energy and the pre-exponential factor. The populations of both ADCSs and compact islands are monitored over a range of temperatures (90–150 °C) with respect to time.

We implement a digital image-processing algorithm in order to extract the ADCS and compact island population distributions from STM images. The algorithm can be summarized by three key steps. First, the height difference between neighboring terraces on the surface (separated by monatomic steps) results in a contrast variation in the gray scale intensity for adspecies on different terraces. A combination of filtering techniques is used to negate this height difference effect as well as to enhance adspecies contrast relative to the surface [34,35]. Second, a mask is created to isolate all of the adspecies on the surface (ADCSs and compact islands), yielding binary filled- and empty-state images [35]. Finally, a classification step is performed to discriminate between ADCSs and compact islands [35]. This is accomplished by employing the fact that ADCSs only appear in empty-state images while compact islands appear in filled- and empty-states.

By plotting the normalized areas of ADCSs and compact islands in pixels as a function of time, the population decay of ADCSs, due to transition to compact islands, is obtained at a variety of temperatures. From the population

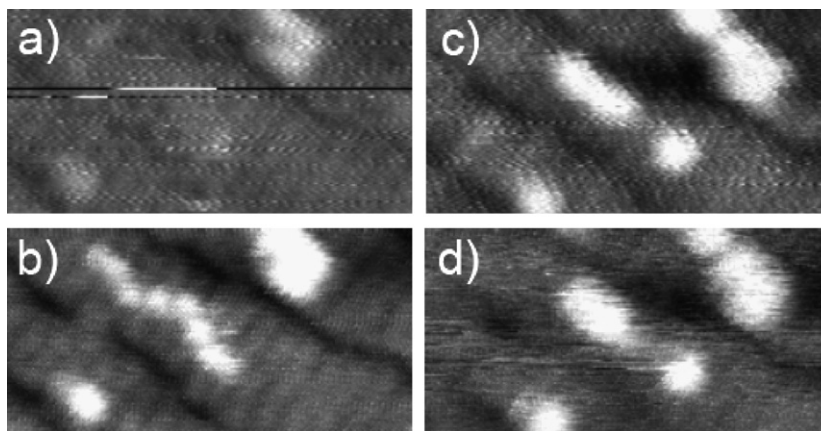


Fig. 4. Filled- and empty-state STM images showing a six-unit ADCS before and after its transition to a compact epitaxial island. (a) Filled-state image (+1.7 V) before conversion, (b) empty-state image (−1.7 V) before conversion, (c) filled-state image after conversion, and (d) empty-state image after conversion. Notice that the surrounding epitaxial islands are visible in both biases before and after.

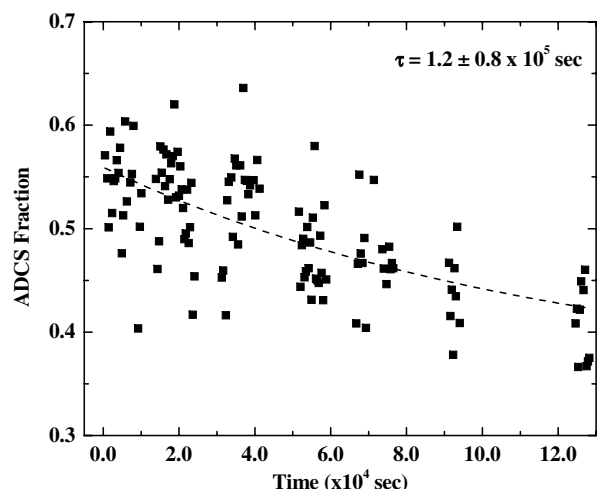


Fig. 5. Time-dependent ADCS population decay data with associated time constant at 90 °C.

decay of ADCSs, we extract a characteristic relaxation time (τ) for each temperature from a first order exponential decay model (see Fig. 5). Each data point in Fig. 5 is based on a $500 \text{ \AA} \times 500 \text{ \AA}$ image. The total number of data points for each temperature ranges from approximately 10 for the highest substrate temperature to 100 for the lowest substrate temperature. We note that not all ADCSs convert to compact epitaxial islands. There is a finite population of unconverted mass. We speculate that the incomplete conversion is caused by the presence of defects, which stabilize some of the ADCSs and prevent their transition to compact islands. The temperature-dependent relaxation times are then fit to a typical Arrhenius-type expression, from which the activation energy is extracted. Fig. 6 shows that the activation energy (E_a) associated with the transition from ADCSs to compact islands is $0.7 \pm 0.2 \text{ eV}$ with a pre-exponential factor (ν_0) on the order of $5 \times 10^{4 \pm 2} \text{ s}^{-1}$.

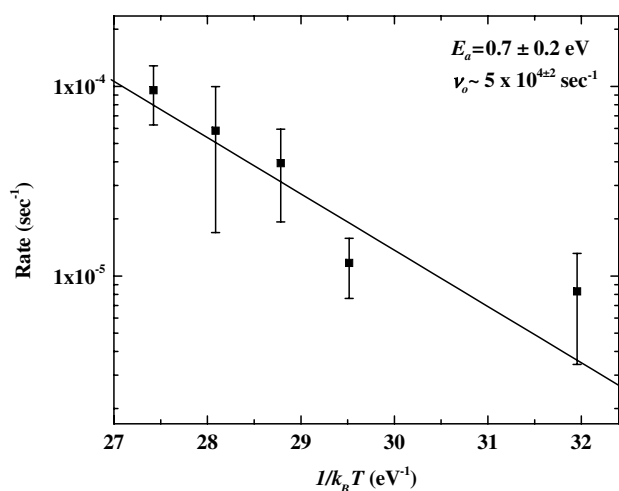


Fig. 6. Arrhenius plot for $90 \text{ °C} \leq T \leq 150 \text{ °C}$ showing activation energy and pre-exponential factor associated with ADCS to compact island transition.

While the activation energy is comparable to experimentally measured values for addimer diffusion [31,36–38] and rotation [26] on Si and Ge surfaces, the attempt frequency is extremely low. Typical values for the attempt frequency are $\sim 10^{13} \text{ s}^{-1}$, on the order of the vibrational frequency of a chemical bond. We surmise that the extremely low pre-factor may reflect the complex nature of the conversion mechanism itself. The mechanism is likely to require a concerted motion of multiple addimers and their interaction with the substrate dimers, as a similar mechanism is predicted for Si homoepitaxy [39]. Further investigation is needed regarding the low pre-factor and its origin.

4. Conclusions

We have identified addimer chain structures (ADCSs) as metastable precursors to the formation of compact epitaxial islands on the Ge–Si(001)-(2 × n) alloyed surface. ADCSs consist of chains of C-dimers residing in adjacent troughs, and extend along all equivalent $\langle 130 \rangle$ directions. The chain length typically ranges from 2 to approximately 12 units. We observe the preferential formation of ADCSs on this surface at room temperature for sub-monolayer Ge deposition. ADCSs exhibit limited mobility on the surface and undergo configurational rearrangements while maintaining $\langle 130 \rangle$ orientations. These ADCSs possess kinked and straight segments. The observed kink-to-straight ratio is close to 2:1, corresponding to a free energy difference of $17 \pm 4 \text{ meV}$. Upon annealing, ADCSs convert to compact islands with an associated activation energy of $0.7 \pm 0.2 \text{ eV}$ and an attempt frequency of $5 \times 10^{4 \pm 2} \text{ s}^{-1}$.

Acknowledgements

The authors thank the National Science Foundation CAREER (DMR-0094145) for their financial support. The above material is also based upon work supported by, or in part by, the US Army Research Laboratory and the US Army Research Office under contract/grant number W911NF-05-1-0012. Sandia is a multiprogram laboratory operated by Sandia Corporation, a Lockheed Martin Company, for the United States Department of Energy's National Nuclear Security Administration under Contract DE-AC04-94AL85000.

References

- [1] D.J. Paul, *Semicond. Sci. Technol.* 19 (2004) R75.
- [2] R.J.P. Lander, Y.V. Ponomarev, J.G.M. van Berkum, W.B. de Boer, *IEEE Trans. Electron Dev.* 48 (2001) 1826.
- [3] O.P. Pchelyakov, Y.B. Bolkhovityanov, A.V. Dvurechenskii, L.V. Sokolov, A.I. Nikiforov, A.I. Yakimov, B. Voigtlander, *Semiconductors* 34 (2000) 1229.
- [4] M. Yoshimi, M. Terauchi, A. Nishiyama, O. Arisumi, A.R. Murakoshi, K. Matsuzawa, N. Shigyo, S. Takeno, M. Tomita, K. Suzuki, Y. Ushiku, H. Tango, *IEEE Trans. Electron Dev.* 44 (1997) 423.

- [5] Y.S. Chieh, J.P. Krusius, D. Green, M. Ozturk, *IEEE Electron Dev. Lett.* 17 (1996) 360.
- [6] S.H. Olsen, A.G. O'Neill, S. Chattopadhyay, K.S.K. Kwa, L.S. Driscoll, D.J. Norris, A.G. Cullis, D.J. Robbins, J. Zhang, *Semicond. Sci. Technol.* 19 (2004) 707.
- [7] P.S. Chen, S.W. Lee, M.H. Lee, C.W. Liu, *Semicond. Sci. Technol.* 21 (2006) 479.
- [8] M.L. Lee, E.A. Fitzgerald, M.T. Bulsara, M.T. Currie, A. Lochtefeld, *J. Appl. Phys.* 97 (2005) 011101.
- [9] O.G. Schmidt, K. Eberl, *IEEE Trans. Electron Dev.* 48 (2001) 1175.
- [10] C.Y. Chen, J.-J. Ho, *IEEE Trans. Electron Dev.* 50 (2003) 1807.
- [11] S. Hazra, A.R. Middy, S. Ray, *J. Phys. D Appl. Phys.* 29 (1996) 1666.
- [12] L. Friedman, G. Sun, R.A. Soref, *Appl. Phys. Lett.* 78 (2001) 401.
- [13] E.A. Fitzgerald, S.B. Samavedam, Y.H. Xie, L.M. Giovane, *J. Vac. Sci. Technol. A* 15 (1997) 1048.
- [14] B. Voigtlander, M. Kastner, *Phys. Rev. B* 60 (1999) R5121.
- [15] R. Butz, S. Kampers, *Appl. Phys. Lett.* 61 (1992) 1307.
- [16] L. Nurminen, F. Tavazza, D.P. Landau, A. Kuronen, K. Kaski, *Phys. Rev. B* 68 (2003) 085326.
- [17] F.-K. Men, C.-R. Hsu, *Phys. Rev. B* 58 (1998) 1130.
- [18] J. van Wingerden, A. van Dam, M.J. Haye, P.M.L.O. Scholte, F. Tuinstra, *Phys. Rev. B* 55 (1997) 4723.
- [19] S. Liu, C.S. Jayanthi, S.-Y. Wu, X. Qin, Z. Zhang, M.G. Lagally, *Phys. Rev. B* 61 (2000) 4421.
- [20] X.R. Qin, M.G. Lagally, *Science* 278 (1997) 1444.
- [21] W. Wulfhekel, B.J. Hattink, H.J.W. Zandvliet, G. Rosenfeld, B. Poelsema, *Phys. Rev. Lett.* 79 (1997) 2494.
- [22] H.J.W. Zandvliet, T.M. Galea, E. Zoethout, B. Poelsema, *Phys. Rev. Lett.* 84 (2000) 1523.
- [23] T.M. Galea, C. Ordas, E. Zoethout, H.J.W. Zandvliet, B. Poelsema, *Phys. Rev. B* 62 (2000) 7206.
- [24] G. Brocks, P.J. Kelly, R. Car, *Surf. Sci.* 269–270 (1992) 860.
- [25] Z. Zhang, F. Wu, H.J.W. Zandvliet, B. Poelsema, H. Metiu, M.G. Lagally, *Phys. Rev. Lett.* 74 (1995) 3644.
- [26] B.S. Swartzentruber, A.P. Smith, H. Jonsson, *Phys. Rev. Lett.* 77 (1996) 2518.
- [27] T. Yamasaki, T. Uda, K. Terakura, *Phys. Rev. Lett.* 76 (1996) 2949.
- [28] G. Brocks, P.J. Kelly, *Phys. Rev. Lett.* 76 (1996) 2362.
- [29] A. van Dam, J. van Wingerden, M.J. Haye, P.M.L.O. Scholte, F. Tuinstra, *Phys. Rev. B* 54 (1996) 1557.
- [30] P.J. Bedrossian, *Phys. Rev. Lett.* 74 (1995) 3648.
- [31] B. Borovsky, M. Krueger, E. Ganz, *Phys. Rev. Lett.* 78 (1997) 4229.
- [32] A.P. Smith, H. Jonsson, *Phys. Rev. Lett.* 77 (1996) 1326.
- [33] Y.-W. Mo, R. Kariotis, B.S. Swartzentruber, M.B. Webb, M.G. Lagally, *J. Vac. Sci. Technol. A* 8 (1990) 201.
- [34] P. Viola, W.M. Wells, *Int. J. Comput. Vision* 24 (1997) 137, The filled- and empty-state images are first registered via maximization of mutual information. This is necessary because a small lateral shift exists between filled- and empty-state images due to piezoelectric tube hysteresis.
- [35] K.R. Castleman, *Digital Image Processing*, Prentice Hall, Upper Saddle River, 1996, The empty-state images are bandpass filtered by convolving with a Laplacian of Gaussian. The purpose of this is two-fold. (i) By differentiating the image twice, the DC component of the Fourier transform is removed. This has the effect of negating the height difference between multiple terraces in the image. (ii) The standard deviation of the Laplacian of Gaussian is set approximately the same as the radius of atoms (2 pixels) to serve as a matched filter. This enhances the contrast of the adspecies (ADCs and compact islands) compared to the background. Third, a mask is created in order to suppress false positive responses at plateau boundaries (i.e., step edges). This is accomplished by thresholding the gradient magnitude of filled- and empty-state images. Fourth, morphological close and open operations are then applied to remove small regions from the binary image representing the product of the thresholded bandpass filtered image and the mask. The above sequence results in binary images of filled- and empty-states, in which only ADCs and compact islands are isolated, while the effects of differing plateau heights, false responses at step edges, and noise are removed. A classification procedure is finally performed to discriminate between ADCs and compact epitaxial islands. Both filled- and empty-state images are used because ADCs only appear in empty-state images. First, a bounding-box is created for all ADCs and compact islands in empty-state images. Next, the centers-of-mass are computed for compact islands in filled-state images. Two criteria are imposed to discriminate ADCs from compact islands. (i) If the center-of-mass of an object in filled-state images lies within a corresponding bounding-box in empty-state images and (ii) if there is no more than a factor of two difference in size, the feature is verified positively as a compact island. If these criteria are not met, the object is identified as an ADC.
- [36] B.S. Swartzentruber, *Phys. Rev. Lett.* 76 (1996) 459.
- [37] M. Krueger, B. Borovsky, E. Ganz, *Surf. Sci.* 385 (1997) 146.
- [38] X.R. Qin, B.S. Swartzentruber, M.G. Lagally, *Phys. Rev. Lett.* 85 (2000) 3660.
- [39] S. Dag, S. Ciraci, C. Kilic, C.Y. Fong, *Surf. Sci.* 479 (2001) 109.